

Distonic Isomers and Tautomers of the Adenine Cation Radical in the Gas Phase and Aqueous Solution

Xiaohong Chen,[†] Erik A. Syrstad,[†] Minh Tho Nguyen,[‡] Pascal Gerbaux,^{*,§} and František Tureček^{*,†}

Department of Chemistry, Bagley Hall, Box 351700, University of Washington, Seattle, Washington 98195-1700, Department of Chemistry, University of Leuven, B-3001 Leuven, Belgium, and Department of Organic Chemistry, University of Mons-Hainaut, Mons, Belgium

Received: July 30, 2004; In Final Form: August 13, 2004

The gas-phase protonation of adenine is predicted to occur preferentially at N₁, N₃, and N₇, which have the highest proton affinities PA = 939, 932, and 904 kJ mol⁻¹, respectively, as calculated by coupled-cluster ab initio theory and combined density functional and Møller–Plesset theory, B3-MP2, with the 6-311++G-(3df,2p) basis set. The collisionally activated dissociation of protonated adenine tautomers at kiloelectronvolt energies in the gas phase proceeds by the loss of a hydrogen atom, which is accompanied by substantial hydrogen migration in the dissociating ion. The product is the adenine cation-radical (**1**^{+•}), which is the most stable C₅H₅N₅^{+•} isomer. The adiabatic and vertical ionization energies of adenine have been calculated to be 8.28 and 8.43 eV, respectively, in excellent agreement with previous photoionization and photoelectron spectroscopy measurements. Structures and relative energies of several isomers of **1**^{+•} (e.g., three imine tautomers and six distonic ions) have been obtained computationally. The imine tautomers are 16–79 kJ mol⁻¹ less stable than **1**^{+•} at 0 K in the gas phase. The distonic ions, in which a hydrogen atom has been shifted from C₂ or C₈ to N₁, N₃, or N₇, are 51–142 kJ mol⁻¹ less stable than **1**^{+•}. Dissociations of protonated adenine tautomers by the loss of H require threshold energies in the range of 381–415 kJ mol⁻¹ and proceed at or close to the thermochemical thresholds. The energy differences between **1**^{+•} and its isomers are diminished to Δ*G*_{298(w)} = 14–121 kJ mol⁻¹ in the polar dielectric corresponding to aqueous solution. However, **1**^{+•} remains the most stable isomer in water. H₉ and the protons of the amino group are calculated to be the most acidic protons in **1**^{+•} (p*K*_a = 3.2–3.3). The deprotonation of the amino group in the ionized adenine moiety in DNA is expected to produce a highly reactive radical that is able to abstract a hydrogen atom from thymine and amino acid residues exothermically.

Introduction

Distonic ions and ylid ions are nonclassical open-shell species in which the charge and radical sites reside on separate atoms.¹ In addition to appearing as intermediates of gas-phase ion dissociations,² distonic and ylid ions are often thermodynamically more stable than their isomeric canonical cation-radical structures, as discovered computationally by Radom and co-workers for distonic isomers of cation radicals of simple aliphatic alcohols, ethers, and amines.³ In contrast, neutral counterparts of distonic and ylid ions are usually transient biradicals and ylids that are as a rule substantially less stable than classical closed-shell molecules for a variety of organic compounds.⁴ A special class of distonic ions that has attracted much attention recently is that derived from aromatic⁵ and heteroaromatic systems. In particular, heteroaromatic distonic and ylid ions have been studied for pyridine,⁶ pyrimidine,⁷ pyrazine,⁸ imidazole,⁹ and thiazole¹⁰ and found to be comparably stable to the canonical cation radicals derived from the ionization of these stable heteroaromatic molecules.

In the course of our study of adenine protonation in the gas phase and by electrospray ionization, we observed that the collisionally activated dissociation (CAD) of protonated adenine yields abundant product cation radicals due to the loss of a hydrogen atom. In addition to violating the even-electron rule of gas-phase ion chemistry,^{11,12} this dissociation raised the question of the structure of the odd-electron products, which could be an adenine cation radical, its tautomers, or nonclassical distonic ions. Whereas tautomers of neutral adenine have been studied in detail by theory,¹³ the properties of cation radicals derived from adenine are much less understood.^{14,15} We now report a combined experimental and computational study of adenine ion dissociations to shed some light on the formation, structures, and stabilities of distonic and ylid ions derived from adenine.

The question of relative stabilities of adenine ion radicals is also relevant to radiation damage of DNA,¹⁶ where direct ionization producing cation radicals and electron capture leading to anion radicals are currently accepted as important mechanisms.¹⁷ We therefore also address by computations the relative free energies and acid–base properties of distonic and tautomeric adenine cation radicals in a polar dielectric such as that existing in aqueous solution.

* Corresponding author. E-mail: turecek@chem.washington.edu. Tel: (206) 685-2041. Fax: (206) 685-3478.

[†] University of Washington.

[‡] University of Leuven.

[§] University of Mons-Hainaut.

Experimental Section

Materials. Adenine (**1**, 99% pure) was purchased from Sigma-Aldrich and used as received. D₂O (99.5% D), acetic acid-*d*₄ (99.5% D), acetone-*d*₆ (99.5% D), and methanol-*d*₄ (99.5% D), all from Cambridge Isotope Laboratories, and methanol (Fisher) were used as received. Anhydrous ND₃ (99% D) was purchased from Matheson.

[N-9-²H, N-10-²H₂]Adenine (**1a**) was prepared by H/D exchange of the labile protons in adenine as follows. Adenine (32 mg) was sonicated to dissolve in 10 mL of D₂O. The solvent was evaporated in vacuo, and the solid was used for measurements.

To prepare [8-²H₁]adenine (**1b**), adenine (1 g) was dissolved in 30 mL of warm D₂O (60–70 °C) containing two drops of acetic acid-*d*₄. The solution was stirred overnight, the solvents were evaporated to dryness in vacuo, and the procedure was repeated twice. A 2-mg aliquot of the solid product was dissolved in 2 mL of methanol, and the solvent was evaporated in vacuo. Mass spectrum (direct probe, 140 °C): *m/z* 136 (M⁺). The deuterium position was assigned from the ¹H NMR spectrum (DMSO-*d*₆, 25 °C) that showed a singlet at δ 8.087. Under the same conditions, adenine gives a narrow singlet at δ 8.088 (H-2) and a broader singlet at δ 8.070 (H-8). The latter band is <5% as intense relative to that of H-2 in the ¹H NMR spectrum of **1b**. The signal assignments are based on the previous study by Laxer et al.,¹⁸ who used extensive ¹⁵N labeling to distinguish the H-2 and H-8 protons through their ¹H-¹⁵N coupling constants.

Measurements. ¹H NMR spectra were taken on a Bruker 300 MHz Avance instrument (Karlsruhe, Germany) in DMSO-*d*₆ at 298 K. Mass spectra were measured on a JEOL HX-110 double-focusing instrument equipped with electron impact and chemical ionization ion sources. Samples were introduced from a direct probe at 130–150 °C. For H/D exchange measurements, the ion source was treated with D₂O at 5×10^{-6} Torr for 30 min before the measurements. Collisionally activated dissociation (CAD) spectra were measured by scanning the electrostatic (E) and magnet (B) analyzers while maintaining a constant B/E ratio (B/E linked scan). Air as the collision gas was admitted to the first field-free region at pressures to achieve 50 and 70% transmittance of the precursor ion beam at 10 keV. Typically, 50–100 scans were collected and averaged to provide the spectra presented here. The mass resolution in the B/E scans was >500. Another set of CAD spectra was measured at 8 keV on the University of Mons large-scale six-sector tandem mass spectrometer as described previously.¹⁹ Oxygen was used as the collision gas at 70% precursor ion beam transmittance.

Calculations

Standard ab initio and density functional theory calculations were performed using the Gaussian 98 and Gaussian 03 suites of programs.^{20a,b} Singlet ion geometries were first optimized with a hybrid functional (B3LYP)²¹ and the 6-31G(d) basis set and then reoptimized with the larger 6-311++G(d,p) basis set. Triplet ion and doublet cation-radical geometries were optimized uniformly with B3LYP and the 6-31+G(d,p) basis set. Spin-unrestricted calculations (UB3LYP and UMP2) were used for open-shell systems. In the UB3LYP calculations, $\langle S^2 \rangle$ operator expectation values ranged from 0.751–0.767 and 0.764–0.766 for doublets and 2.00–2.02 for triplets. Contamination by higher spin states in UMP2 calculations was treated by a standard annihilation procedure.²² Optimized structures were characterized by harmonic frequencies as local minima (all real frequencies) and saddle points (one imaginary frequency). The calcu-

lated frequencies (scaled by 0.963) and moments of inertia were used to calculate 298 K enthalpies and entropies using the rigid rotor–harmonic oscillator approximation. The optimized geometries are available as Supporting Information; the harmonic frequencies can be obtained from the corresponding author upon request. Dissociation pathways were studied by changing one internal coordinate in 0.1-Å steps while fully optimizing the other internal coordinates. Improved energies were obtained by single-point calculations that combined B3LYP and spin-projected MP2 energies calculated with the 6-311++G(2d,p) basis set according to eq 1.

$$E(\text{B3-PMP2}) = 0.5[E(\text{B3LYP}) + E(\text{PMP2})] \quad (1)$$

These calculations, which are denoted as B3-PMP2,²³ have been shown previously by us and others²⁴ to provide improved accuracy for several closed-shell and open-shell systems of medium (10–50 atoms) size.²⁵ Further expansion of the basis set by adding shells of d and f functions on carbon and nitrogen atoms and including two shells of p functions on hydrogens, 6-311++G(3df,2p), resulted in B3-PMP2 relative energies that were very similar (within ± 5 kJ mol⁻¹) to those calculated with B3-PMP2/6-311++G(2d,p). This is consistent with our previous study of basis set effects in an aromatic system.²⁶ For selected systems, we carried out coupled-cluster²⁷ single-point energy calculations with single, double, and perturbational triple excitations, CCSD(T),²⁸ using the 6-31G(d,p) basis set. These were extrapolated to the larger basis sets in the usual fashion.²⁶ Population analyses were performed with the 6-311++G(2d,p) basis set using the natural population analysis (NPA) formalism.²⁹ In contrast to Mulliken population analysis, NPA gave very reasonable spin populations that showed only minor polarization effects in inverted spin populations at atoms adjacent to those with high spin densities.

Complete active space (CASSCF) calculations³⁰ of the reaction path in N-1-protonated adenine 2⁺ were carried out with the 6-31++G(d,p) basis set. The active space consisted of placing six electrons in three occupied and three virtual in-plane σ - and *n*-type orbitals that were identified by population analysis of the wave function in 2⁺.

Solvation free energies were calculated by B3LYP/6-31+G-(d,p) using the self-consistent reaction field polarizable continuum models (PCM) included in Gaussian 98^{31a} and Gaussian 03.^{31b} Structures were reoptimized by PCM-B3LYP/6-31+G-(d,p) using standard parameters (water dielectric constant; atomic and van der Waals radii) included in Gaussian 98.

Results

Protonated Adenine Tautomers. Adenine exists as a single canonical isomer (**1**) in the gas phase and aqueous solution, as corroborated by theoretical calculations of the relative energies for the complete set of 14 possible tautomers, out of which structure **1** is thermodynamically the most stable.¹³ Although the protonation of adenine in aqueous solution occurs mostly at N₁,³² gas-phase protonation under the conditions of chemical ionization (CI) is expected to depend critically on the topical proton affinities of the individual basic centers in the molecule.³³ Figure 1 shows the B3-MP2 and CCSD(T) calculated topical proton affinities that indicate very similar basicity for N₁ and N₃ (PA = 939 and 932 kJ mol⁻¹, respectively). The third most basic center is N₇ (PA = 904 kJ mol⁻¹), whereas the amino group (PA = 846 kJ mol⁻¹) is somewhat less basic and the carbon positions are only weakly basic. The calculated topical proton affinity for the most basic site N₁ is in acceptably good agreement with the tabulated experimental value (943 kJ

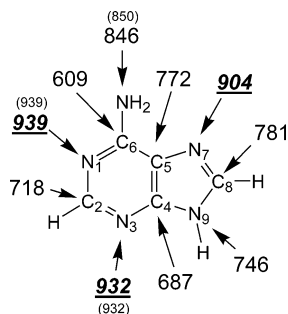


Figure 1. B3-MP2/6-311++G(3df,2p)-calculated typical proton affinities at 298 K in adenine. The small-font numbers in parentheses are from effective CCSD(T)/6-311++G(3df,2p) calculations, including zero-point and 298 K enthalpy corrections.

mol^{-1})³⁴ and previous MP4 calculations.³⁵ The very similar typical proton affinities at N₁ and N₃ virtually preclude the selective protonation of either position to be achieved in the gas phase, which can be expected to produce mixtures of tautomeric cations **2⁺** and **3⁺** even if carried out with a very mild acid of a matching proton affinity. On protonation with common gas-phase acids (e.g., NH₄⁺, PA(NH₃) = 853 kJ mol⁻¹, as used in ammonia CI), N₁, N₃, and N₇ can be expected to be attacked, giving rise to tautomeric cations **2⁺**, **3⁺**, and **4⁺** (Scheme 1).

The proportions of these ions depend on the experimental conditions. Proton transfer in the gas phase is known to occur at the collisional frequency for reactions that have $\Delta G^{\circ}_T < -40$ kJ mol⁻¹.³⁶ Hence, under kinetic control, **2⁺**, **3⁺**, and **4⁺** should be formed in nearly equimolar (0.33) fractions. However, because protonated adenine can react with neutral adenine molecules that are present in the ion source, less stable ions **3⁺** and **4⁺** can be depleted to form the most stable tautomer **2⁺**. Under proton-transfer equilibrium conditions at 473 K, we calculate the relative ΔG°_{473} for **2⁺**, **3⁺**, and **4⁺** to be 0.0, 7.5, and 30.6 kJ mol⁻¹, respectively, leading to the respective equilibrium molar fractions equal to 0.87, 0.13, and <0.01. The kinetically controlled and equilibrium molar ratios represent the two extremes of ion populations for **2⁺**, **3⁺**, and **4⁺**. Note that the partial pressure of adenine in the ion source is low (typically $2-3 \times 10^{-6}$ Torr) and cannot be substantially increased because of severe source contamination and ensuing arcing problems.

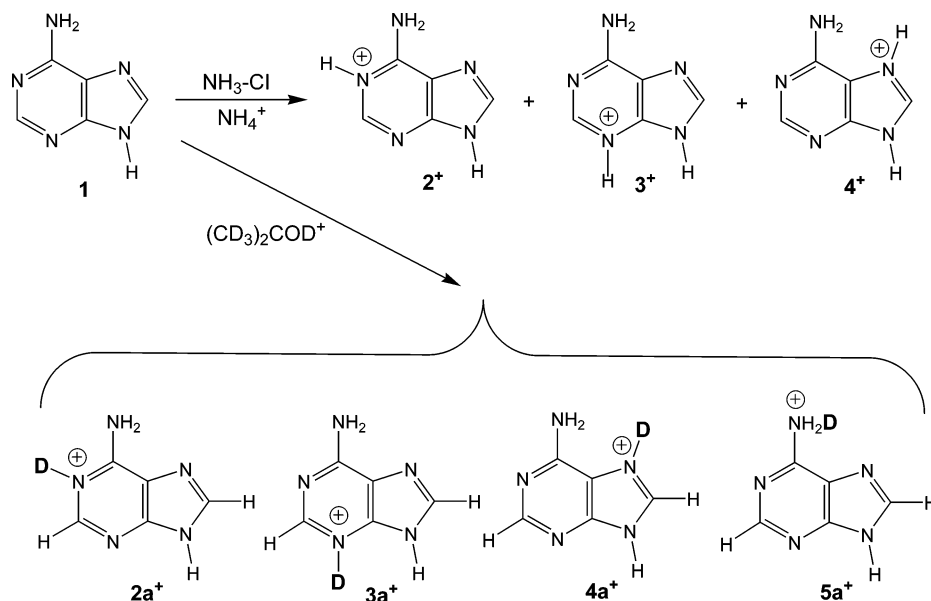
Under these conditions, proton-transfer collisions between adenine and **3⁺** or **4⁺** are unlikely.

Owing to their short residence time in the ion source (<10 μs), ions **2⁺**, **3⁺**, and **4⁺** undergo collisions mainly with molecules of the chemical ionization gas, which, however, cannot result in tautomer equilibration because the reverse proton transfer is endothermic. For example, the 473 K free energies for proton transfer to ammonia from **3⁺** and **4⁺** are calculated to be 69 and 45 kJ mol⁻¹, respectively, leading to the respective equilibrium constants of $K_{\text{eq},473} = 2.7 \times 10^{-8}$ and 1.2×10^{-5} . Because ions **3⁺** and **4⁺** undergo on average 70–100 collisions with the CI gas molecules before leaving the ion source, the probability of reverse proton transfer is negligibly small.

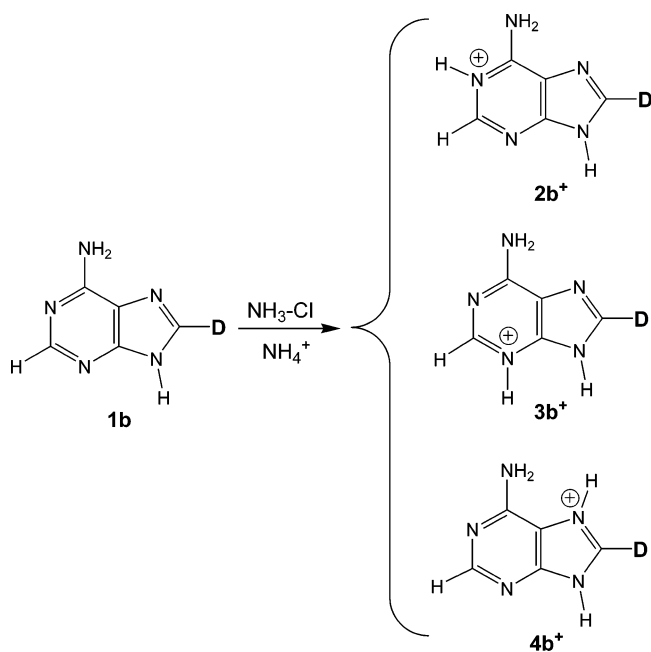
The protonation and D-labeling schemes used in this work relied on a combination of H⁺/D⁺ transfer and H/D exchange (Schemes 1–4) that we developed previously to generate uracil cations.³⁷ Deuteration with (CD₃)₂COD⁺ results in single deuteron incorporation because acetone-*d*₆ does not promote H/D exchange with the labile N₉-H and NH₂ protons in adenine (Scheme 1). The negligible level of exchange in acetone-*d*₆ and acetone-*d*₆-CI is due to the fact that acetone is a weak Lewis base in the gas phase that does not engage readily in surface-catalyzed proton exchange. However, because of the acidity of these reagents (PA(acetone) = 812 kJ mol⁻¹), they can attack positions N₁, N₃, N₇, and the amino group, giving rise to an even richer mixture of tautomeric cations. Protonation with NH₄⁺/NH₃ and deuteration with ND₄⁺/ND₃ proceed under conditions where the acidic protons at N₉ and in the NH₂ group are exchanged and cannot be labeled selectively. However, the C-2 and C-8 protons are inactive in ammonia-CI in the gas phase, so protonation with NH₄⁺/NH₃ of C₈-labeled adenine **1b** forms cations **2b⁺**–**4b⁺** (Scheme 2). A combination of H/D exchange in solution with gas-phase protonation under nonexchanging conditions produced ions **2c⁺**–**5c⁺** (Scheme 3). Finally, complete H/D exchange and gas-phase deuteration yielded ions **2d⁺**–**4d⁺**.

In summary, the gas-phase protonation of adenine is non-selective and leads to the formation of 2 or 3 of the most stable tautomeric ions, as shown in Schemes 1–4. To generate pure tautomers, one has to resort to protonation in solution, as applied in electrospray ionization,³⁸ or rely on ion–molecule reactions such as chlorine or bromine substitution with ammonia in

SCHEME 1



SCHEME 2



6-chloro- or bromopurine.³⁹ Nevertheless, useful information on ion properties can be obtained from CI mass spectra by combining different isotope-labeling strategies.

Collisionally Activated Dissociation of Protonated Adenine Tautomers. The CAD spectra of protonated adenine show three types of dissociations: (1) loss of a hydrogen atom (m/z 135), (2) loss of ammonia (m/z 119), and (3) ring cleavage dissociations with consecutive eliminations of HCN (m/z 109), CH_2N_2 (m/z 67), and other highly unsaturated fragments in combination with further dehydrogenation (Figure 2). That most of the ring-cleavage fragmentations originate from protonated adenine is supported by the CAD spectrum of the adenine cation radical (**1⁺**, m/z 135, spectrum not shown), which displays only one major fragment at m/z 108 due to the loss of HCN. Interestingly, the loss of H is the dominant dissociation of protonated adenine despite the fact that it violates the even-electron rule of gas-phase ion chemistry.^{11,12} Because there are six different

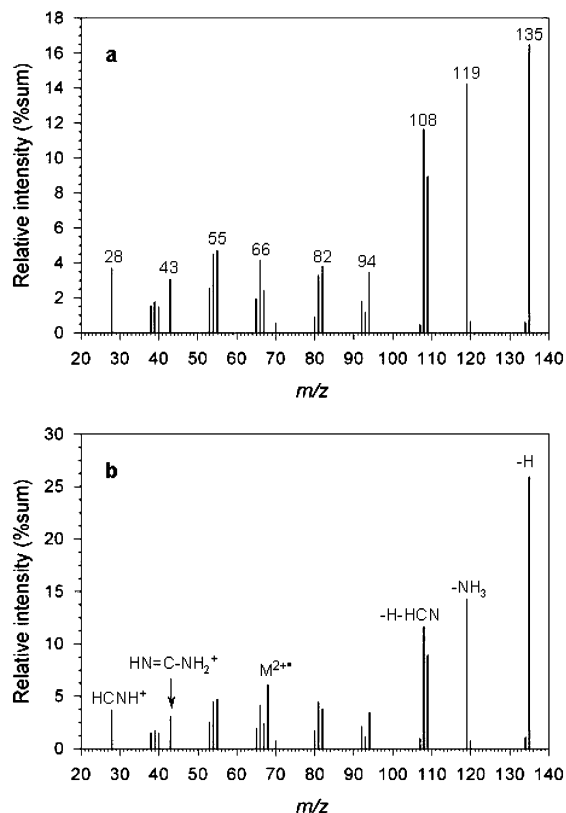
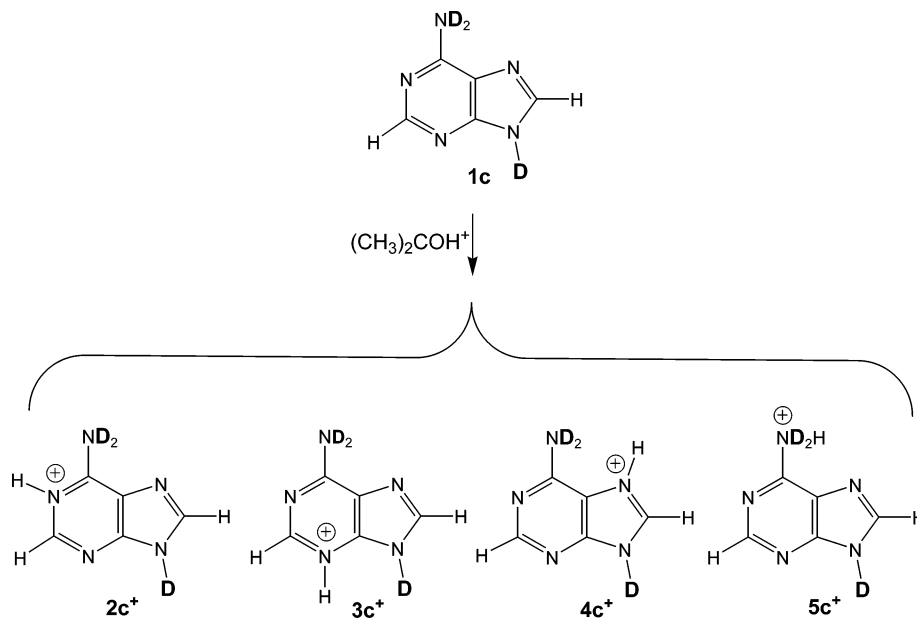


Figure 2. B/E linked scan collisionally activated dissociation spectra (CAD) of protonated adenine, m/z 136. (a) Ions (8 keV) from protonation with $(\text{CH}_3)_2\text{COH}^+$ in acetone-CI, O_2 as the collision gas at 70% precursor ion beam transmittance. (b) Ions (10 keV) from protonation with NH_4^+ in NH_3 -CI, air as the collision gas at 50% precursor ion beam transmittance.

hydrogen atoms in each protonated adenine tautomer, the loss of H can in principle result in the formation of a multitude of isomeric cation radicals with the $\text{C}_5\text{H}_5\text{N}_5^{+\bullet}$ composition. We attempted to deconvolute the mixture by analyzing the CAD spectra of deuterium-labeled ions as shown in Figures 3 and 4. The major dissociations by loss of H or D and ammonia isotopomers are summarized in Table 1.

SCHEME 3



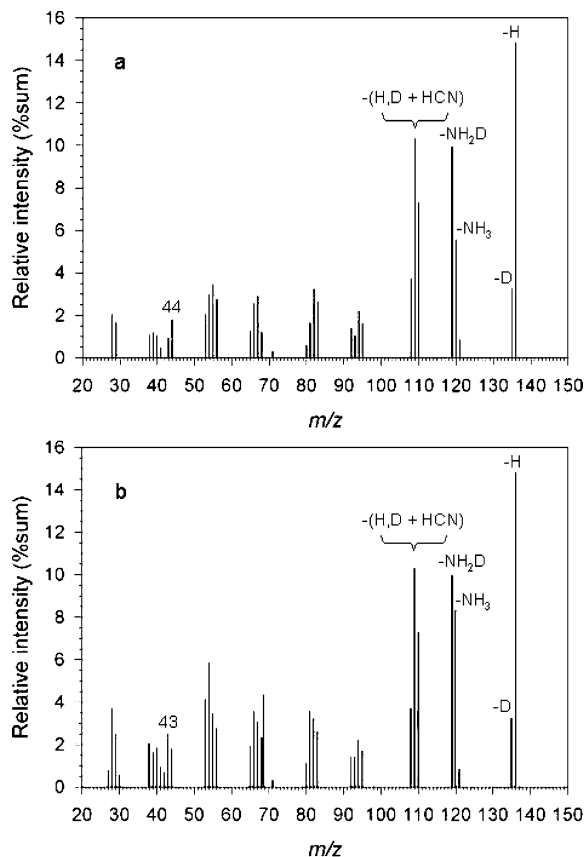
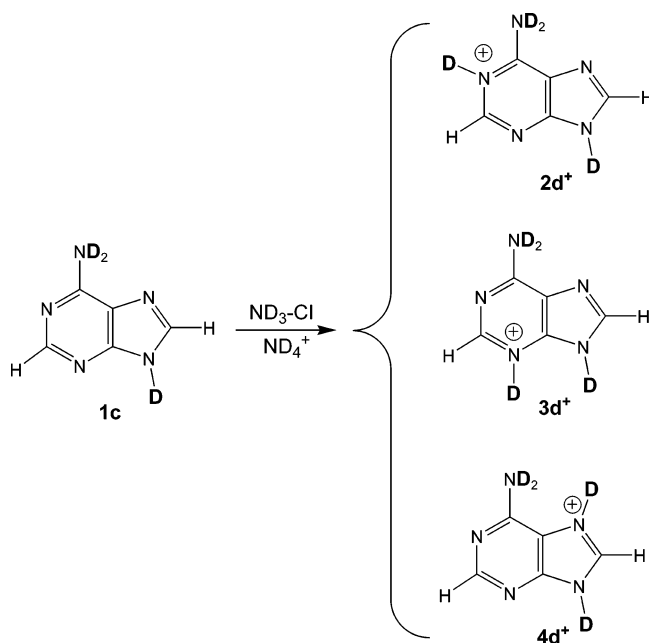


Figure 3. B/E linked scan CAD spectra of (a) (M + D)⁺ ion (*m/z* 137) from (CD₃)₂CO⁺ deuteration of adenine in acetone-d₆-Cl. 8 keV, O₂ as the collision gas at 70% precursor ion beam transmittance. (b) (M + H)⁺ ion (*m/z* 137) from NH₄⁺ protonation of [8-²H₁]adenine in NH₃-Cl. 10 keV, air as the collision gas at 50% precursor ion beam transmittance.

SCHEME 4



Both of these dissociations show nonrandom losses of labeled neutral fragments. The loss of ammonia from 2a⁺–5a⁺ and 2b⁺–4b⁺ shows the preferential involvement of the ionizing proton that must be transferred from the protonation site (N₁, N₃, or N₇) on the amino group. Although we did not label the amine nitrogen atom to establish unambiguously its loss as

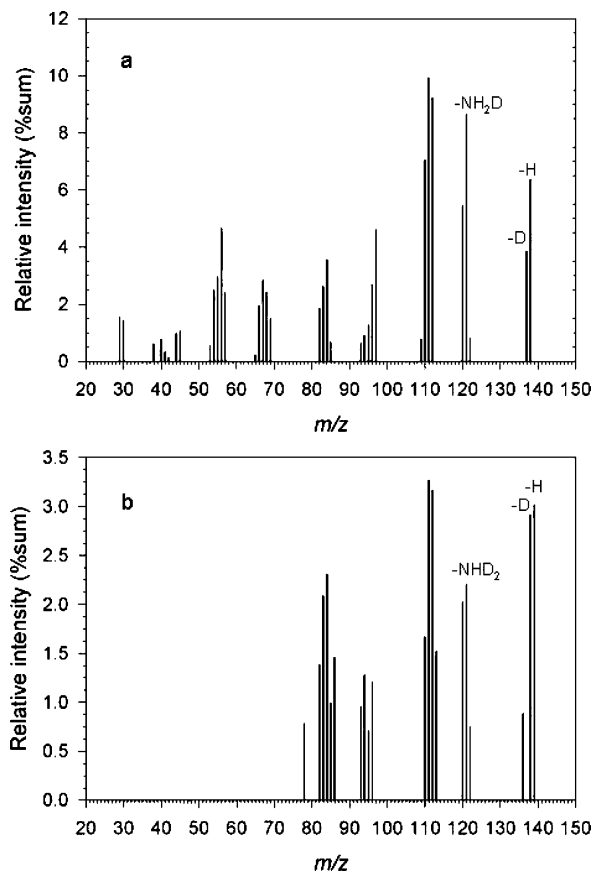


Figure 4. B/E linked scan CAD spectra of (a) the (M + H)⁺ ion (*m/z* 139) from (CH₃)₂COH⁺ protonation of [9,10,10-²H₃]adenine in acetone-Cl. 8 keV, O₂ as the collision gas at 70% precursor ion beam transmittance. (b) (M + D)⁺ ion (*m/z* 140) from ND₄⁺ deuteration of [9,10,10-²H₃]adenine in ND₃-Cl. 10 keV, air as the collision gas at 50% precursor ion beam transmittance.

TABLE 1: Product Ion Distributions in the CAD Spectra

| precursor ion | loss of | | | loss of | | | | |
|----------------------------------|---------|---|--------|-----------------|-------------------|------------------|-----------------|------------|
| | H | D | random | NH ₃ | NH ₂ D | NHD ₂ | ND ₃ | random |
| 2a ⁺ –5a ⁺ | 5.1 | 1 | 5:1 | 36 | 64 | | | 50:50:0:0 |
| 2b ⁺ –4b ⁺ | 6.2 | 1 | 5:1 | 89 | 11 | | | 50:50:0:0 |
| 2c ⁺ –5c ⁺ | 1.7 | 1 | 1:1 | 4 | 37 | 59 | | 5:45:45:5 |
| 2d ⁺ –4d ⁺ | 1.1 | 1 | 0.75:1 | | 13 | 45 | 42 | 0:20:60:20 |

ammonia, energy calculations (vide infra) indicate it to be the lowest-energy and thus the most probable dissociation channel. The CAD spectrum of 2c⁺–5c⁺ indicates some exchange involving protons from C₂ and C₈ that lower the fraction of NHD₂ (59%), although it exceeds the statistical value of 45% (Table 1). Some of this hydrogen transfer originates from C₈, as documented by the 11% fraction of NH₂D lost from 2b⁺–4b⁺. The deuteration of 1c results in an enhanced loss of ND₃ in the CAD spectrum of ions 2d⁺–4d⁺ (42%), although exchange with protons from C₂ and C₈ manifests itself by the substantial fraction for loss of NHD₂ (45%).

The loss of H and D appears to show a nearly statistical distribution in the CAD spectra of 2a⁺–5a⁺ and 2b⁺–4b⁺, taking into account the fact that the loss of D could be disfavored by isotope effects. However, the loss of H is preferred from 2c⁺–5c⁺ where the ionizing agent was a proton but less so in 2d⁺–4d⁺ where the ionizing agent was a deuteron. These data are incompatible with a *complete* scrambling of all six hydrogens in protonated adenine and indicate some, albeit low, level of specificity in the formation of the C₅H₃N₅⁺ product ions. However, an experimental study of these ions is difficult because

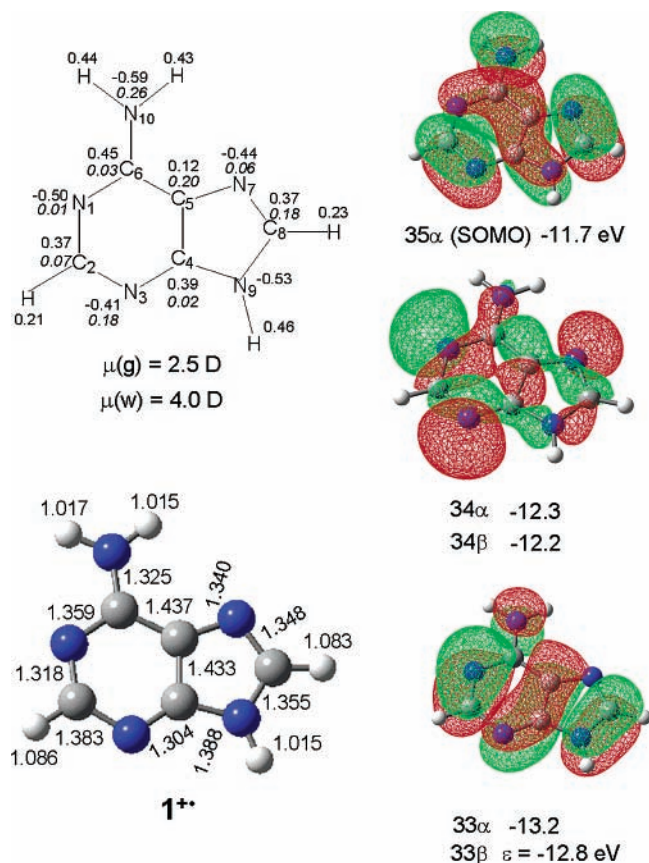


Figure 5. (Bottom left) B3LYP/6-31+G(d,p) optimized structure of $1^{+\bullet}$ with bond lengths in angstroms. (Top left) Atomic charges (roman numerals), spin densities (italics), and dipole moments in units of Debye in the gas phase, $\mu(g)$, in aqueous solution $\mu(w)$. (Right) molecular orbitals with orbital energies in electronvolts.

(1) only one tautomer of adenine is stable and thus accessible to experimental study and (2) its CAD spectrum is not very informative. We have therefore resorted to a computational analysis of the dissociations of protonated adenine with the goal of identifying plausible structures for $C_5H_5N_5^{+\bullet}$ product ions and also investigating the dissociation pathways at adequately high levels of theory.

Adenine Cation Radicals in the Gas Phase. In this section, we present the results of geometry optimizations of several isomers of the adenine cation radical and discuss their relative energies.

Of the multitude of possible isomers, of particular interest are those that can be produced by hydrogen atom loss from the most stable cations $2^+ - 5^+$.

Ion $1^{+\bullet}$ shows structure features that resemble those of the neutral molecule (Figure 5).^{13,14} The bicyclic skeleton in $1^{+\bullet}$ is essentially planar, as in adenine, and the amino group shows less pyramidization. The latter feature may be an artifact of the DFT optimization procedure, as noticed previously.⁴⁰ Compared to **1**, the optimized structure of $1^{+\bullet}$ shows interesting alternating changes in the skeletal bond lengths, $\Delta(\text{Å})$ (e.g., -0.023 , $+0.049$, -0.032 , $+0.037$, $+0.028$, -0.028 , -0.044 , $+0.040$, -0.025 , $+0.010$) for the changes upon ionization in the lengths of the N_1-C_2 , C_2-N_3 , N_3-C_4 , C_4-C_5 , C_5-C_6 , C_6-N_{10} , C_5-N_7 , N_7-C_8 , C_8-N_9 , and C_4-N_9 bonds, respectively. These correlate with the electronic structure of $1^{+\bullet}$, which shows ionization occurring mainly from a frontier π orbital ($35\alpha\beta$, HOMO in **1** becoming the SOMO in $1^{+\bullet}$) that has nodal surfaces intersecting the N_1-C_2 , N_3-C_4 , C_8-N_9 , C_5-N_7 , and C_6-N_{10} bonds (Figure 5).¹⁴ Removing one electron from this orbital

TABLE 2: Relative Energies of Adenine Cation Radicals

| species | relative energy ^a | | | | |
|-----------------|------------------------------|-----------------------|-----------------------|-----------------------|---------------------------|
| | $\Delta H_0(g)^b$ | $\Delta H_{298}(g)^c$ | $\Delta G_{298}(g)^d$ | $\Delta G_{298}(w)^e$ | ΔG_{sol}^f |
| $1^{+\bullet}$ | 0 | 0 | 0 | 0 | -268 |
| $6^{+\bullet}$ | 16 (17) ^g | 16 | 17 | 14 | -270 |
| $7^{+\bullet}$ | 79 (82) ^g | 79 | 78 | 43 | -303 |
| $8^{+\bullet}$ | 46 (51) ^g | 45 | 46 | 20 | -293 |
| $9^{+\bullet}$ | 51 (54) ^g | 52 | 51 | 38 | -283 |
| $10^{+\bullet}$ | 77 | 77 | 77 | 63 | -283 |
| $11^{+\bullet}$ | 50 (54) ^g | 50 | 50 | 39 | -279 |
| $12^{+\bullet}$ | 84 | 83 | 82 | 68 | -282 |
| $13^{+\bullet}$ | 73 | 74 | 72 | 38 | -303 |
| $14^{+\bullet}$ | 142 | 143 | 147 | 121 | -294 |

^a In units of kJ mol^{-1} . ^b Relative energies (0 K) in the gas phase from B3-PMP2/6-311++G(3df,2p) single-point energies and B3LYP/6-31+G(d,p) zero-point corrections. ^c Relative enthalpies (298 K) in the gas phase. ^d Relative free energies (298 K) in the gas phase. ^e Relative free energies (298 K) in water. ^f PCM solvation energies of ions optimized in the water dielectric. ^g From effective CCSD(T)/6-311++G(3df,2p) calculations and B3LYP/6-31+G(d,p) zero-point corrections.

decreases the π -antibonding interaction in these bonds and results in their shortening. Conversely, the C_2-N_3 , C_4-N_9 , C_4-C_5 , C_5-C_6 , and N_7-C_8 bonds, where the $35\alpha\beta$ π orbital is bonding, are weakened and elongated by ionization. The calculated adiabatic ionization energy of adenine, $IE_{\text{adiab}} = 8.28$ eV, is practically identical to the experimental value from photoionization measurements (8.26 ± 0.03 eV),⁴¹ and very good agreement is also found for the calculated vertical ionization energy, $IE_{\text{vert}} = 8.43$ eV, and the experimental values from photoelectron spectra (8.44 ⁴² and 8.48 eV⁴³). We note that recent bracketing measurements of electron transfer reported IE_{adiab} of adenine to be close to 8.55 eV,⁴⁴ which agrees neither with our calculations nor with the previous photoionization measurements.⁴² The reason for this disagreement is not clear.⁴⁵

N_1 -protonated imine tautomer $6^{+\bullet}$ is the second most stable isomer among adenine cation radicals. The ion shows an interesting distortion of the imine group that opens the $N_{10}-C_6-C_5$ angle to 131.3° and increases the $H_{10}-N_7$ distance to 2.837 Å (Figure S1, Supporting Information). N_3 and N_7 -protonated imines $7^{+\bullet}$ and $8^{+\bullet}$ (Figure S2, Supporting Information) are 79 and 45 kJ mol^{-1} less stable than $1^{+\bullet}$, respectively, in the gas phase at 298 K, and their relative stabilities are comparable to those of distonic ions $9^{+\bullet}-13^{+\bullet}$ (Table 2). The least stable isomer of this set is N_7 -protonated C_8 -ylid ion $14^{+\bullet}$, which is 140 kJ mol^{-1} less stable than $1^{+\bullet}$ in the gas phase. The ion structures are presented in Figures 6 and S3 and S4 (Supporting Information), and their most salient features are briefly discussed here. Distonic ions $9^{+\bullet}-13^{+\bullet}$ show substantial shortening of the C-N bonds between the hydrogen-deficient carbon atoms and the imine nitrogens. For example, the C_2-N_3 bond in $9^{+\bullet}$ (1.261 Å, Figure 6) is substantially shorter than the same bond in $1^{+\bullet}$ (1.383 Å), and analogous shortening is observed for the C_8-N_9 bond in $10^{+\bullet}$, the C_2-N_1 bond in $11^{+\bullet}$, the C_8-N_9 bond in $12^{+\bullet}$, and the C_2-N_3 bond in $13^{+\bullet}$. This shortening indicates increased bond orders so that the affected CN bonds acquire partial triple-bond character.

Despite the similar relative energies of the imine and distonic ion isomers, there are substantial differences in their electron distributions that are relevant to their ion chemistry. A common feature of the classical structures $1^{+\bullet}$, $6^{+\bullet}$, $7^{+\bullet}$, and $8^{+\bullet}$ is that all have a singly occupied molecular orbital (SOMO) that is a uniformly delocalized π orbital that shows nodes dissecting the N_1-C_2 , N_3-C_4 , C_4-N_9 , C_5-N_7 , and C_6-N_{10} bonds (Figures 5 and S1). However, a closer analysis shows that the ions do

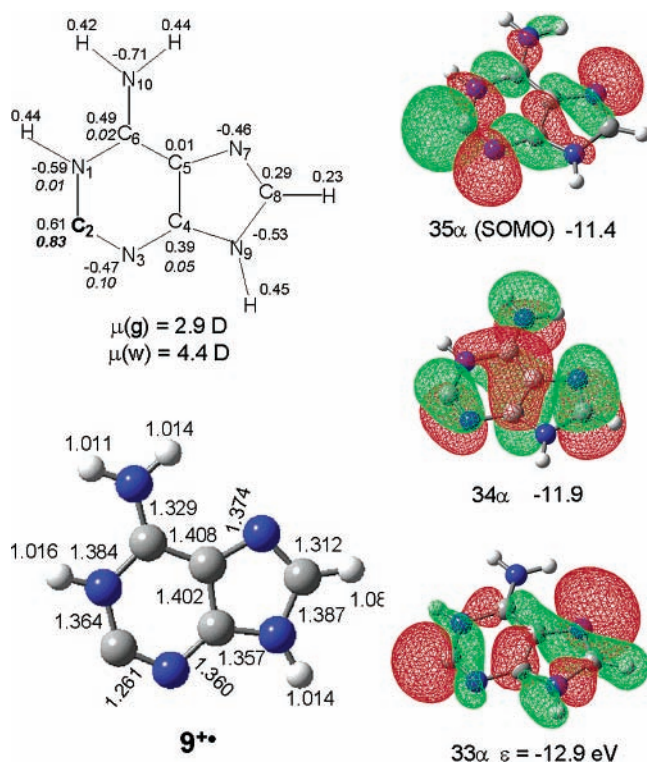


Figure 6. B3LYP/6-31+G(d,p)-optimized structure of $9^{+\bullet}$. Description the same as in Figure 5.

differ in the α and β spin-orbital manifolds and also in the way the spin density is distributed among the ring atoms and the amino or imino groups. Figure 5 shows that the electron spin density in $1^{+\bullet}$ is delocalized over the entire ion with major accumulations at N₃, C₅, C₈, and N₁₀. The SOMO (35α) energy (-11.70 eV) is separated from those of the underlying 34α and 34β orbitals (-12.30 and -12.24 eV, respectively, Figure 5). Imine ions $6^{+\bullet}$, $7^{+\bullet}$, and $8^{+\bullet}$ show somewhat greater odd-electron localization at the imine nitrogen (N₁₀), which accounts for 50, 58, and 65%, respectively, of the spin density, and the rest is delocalized among N₃, C₈, and C₅ (Figure S1). The greater spin localization at N₁₀ in $6^{+\bullet}$, $7^{+\bullet}$, and $8^{+\bullet}$ is due to the polarization of the β -orbital manifolds that show increased energies for the 34β and 33β orbitals compared to their 34α and 33α counterparts. Note that the $33\alpha\beta$ and $34\alpha\beta$ orbitals are in-plane combinations of the lone-pair atomic orbitals at N₁, N₃, N₇, and N₁₀, so spin polarization in 34β and 33β results in increased spin density on the involved nitrogen atoms.

Compared to the classical structures $1^{+\bullet}$, $6^{+\bullet}$, $7^{+\bullet}$, and $8^{+\bullet}$, the distonic ions $9^{+\bullet}$ – $14^{+\bullet}$ show predominant (80–90%) spin localization at the carbon atoms lacking the hydrogen atom (C₂ and C₈) as shown for $9^{+\bullet}$ (Figure 6). These carbon atoms also carry substantial positive charge in the relevant cation radicals (e.g., 0.61 at C₂ in $9^{+\bullet}$, 0.61 at C₈ in $10^{+\bullet}$, and likewise for the other distonic and ylid ions). Somewhat deceptively, population analysis with spin-unrestricted wave functions showed the highest singly occupied molecular orbital (35α , SOMO) in $9^{+\bullet}$, $10^{+\bullet}$, $11^{+\bullet}$, $12^{+\bullet}$, and $14^{+\bullet}$ to be a delocalized π orbital. However, a closer inspection of the frontier orbitals and population analysis in the restricted open-shell formalism revealed that the 35α SOMOs were all antibonding combinations of an in-plane p orbital on the hydrogen-deficient carbon atom and the σ orbitals of the pyrimidine or imidazole rings (Figure 6). The charge and spin localization on the hydrogen-deficient carbon atoms in $9^{+\bullet}$ – $14^{+\bullet}$ suggests that these ions can be viewed

TABLE 3: Ion Dissociation Energies

| ion reactant | products | $\Delta H_{\text{rxn},0}^{a,b}$ | | | |
|--------------|----------------------------|---------------------------------|----------------------|------------------|----------------------|
| | | 6-311++G(2d,p) | | 6-311++G(3df,2p) | |
| | | B3-PMP2 | CCSD(T) ^c | B3-PMP2 | CCSD(T) ^c |
| 2^+ | $1^{+\bullet} + \text{H}$ | 408 | 406 | 415 | 415 |
| | $6^{+\bullet} + \text{H}$ | 424 | 421 | 432 | 432 |
| | $9^{+\bullet} + \text{H}$ | 463 | 464 | 466 | 470 |
| | $10^{+\bullet} + \text{H}$ | 488 | | 491 | |
| | $15^+ + \text{NH}_3$ | 371 | | 374 | |
| 3^+ | $1^{+\bullet} + \text{H}$ | 401 | 399 | 408 | 408 |
| | $7^{+\bullet} + \text{H}$ | 479 | 478 | 487 | 490 |
| | $11^{+\bullet} + \text{H}$ | 455 | 457 | 458 | 462 |
| | $12^{+\bullet} + \text{H}$ | 489 | | 492 | |
| 4^+ | $1^{+\bullet} + \text{H}$ | 373 | 371 | 381 | 381 |
| | $8^{+\bullet} + \text{H}$ | 418 | 419 | 427 | 433 |
| | $13^{+\bullet} + \text{H}$ | 452 | | 454 | |
| | $14^{+\bullet} + \text{H}$ | 513 | | 523 | |

^a In units of kJ mol^{-1} . ^b From B3-PMP2 single-point energy calculations with the indicated basis sets and including B3LYP/6-31+G(d,p) zero-point energy corrections. ^c Effective energies from basis set expansions, $E[\text{CCSD(T)/large basis set}] = E[\text{CCSD(T)/6-31G(d,p)}] + E[\text{PMP2/large basis set}] - E[\text{PMP2/6-31G(d,p)}]$.

as ionized carbenes rather than distonic ions with separated charge and spin.

Bond Dissociations in Adenine Cations. The previous analysis of the ion electronic properties is relevant to the understanding of the unimolecular ion dissociations. The calculated threshold energies point to the elimination of ammonia as the lowest-energy channel that requires $\Delta H_{\text{rxn},0} = 371$ kJ mol^{-1} to produce the purin-6-yl cation (15^+). This is consistent with the predominance of the purinyl cation (m/z 109) in the CAD spectra obtained at low collision energies.⁴⁶ Loss of a hydrogen atom from cations 2^+ – 4^+ is substantially endothermic (Table 3).

The calculated product threshold energies suggest that the classical adenine structure $1^{+\bullet}$ should be favored as a product of H atom loss from all tautomeric adenine cations. However, a comparison of the electronic structures of the reactants and $1^{+\bullet}$ indicates that the cleavage of the N–H bonds may involve an additional energy barrier. This follows from the fact that whereas the N–H bonds in the cations are in the plane of the purine ring and can interact with the σ -electron framework homolytic cleavage of the N–H bonds requires placing an odd electron in the SOMO in $1^{+\bullet}$, which is a π orbital. This implies that the dissociating ion must undergo electron reorganization that requires mixing of the σ and π orbitals along the dissociation path. The question is whether such reorganization results in a substantial energy increase above the dissociation threshold.

Dissociations of the C₂–H and C₈–H bonds leading to the corresponding distonic cation radicals pose similar questions. The SOMOs in the distonic ions are σ -type orbitals (35α) that are nearly degenerate with the highest occupied π orbitals (34α). This degeneracy can cause complications in the homolytic dissociation of the C–H bond, where the unpaired electron in the adenine cation radical can interact with the σ and π orbitals, resulting in an energy increase.

To answer these questions, we investigated the potential energy surfaces for N₁–H and C₂–H bond dissociations in 2^+ , N₃–H bond dissociation in 3^+ , and N₇–H and C₂–H bond dissociations in 4^+ . We note that homolytic and heterolytic bond dissociations in closed-shell systems are potentially difficult to study by computations using single-determinant wave functions,⁴⁷ although less is known about the performance of DFT methods in such cases. Figure 7a shows the potential energy

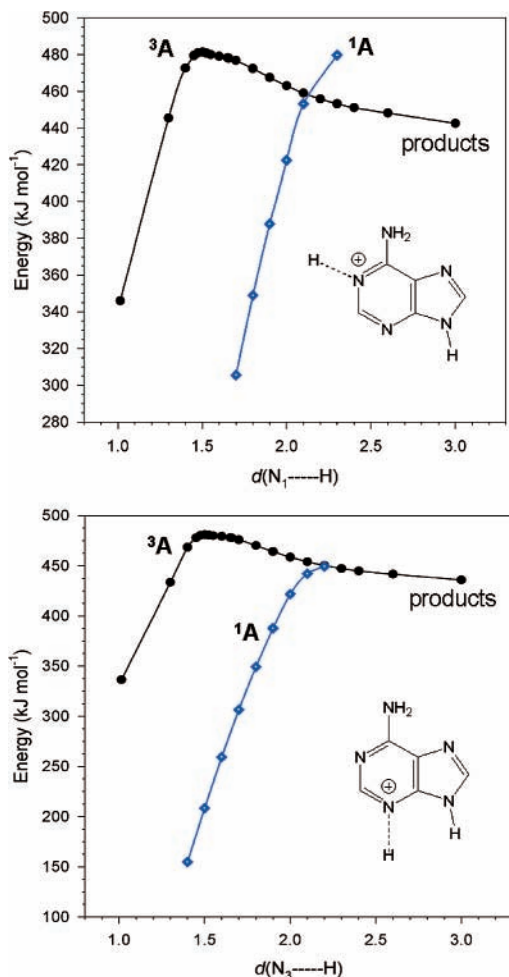


Figure 7. Potential energy profiles along the N-H bond dissociations in (a, top) 2⁺ and (b, bottom) 3⁺.

surface (PES) along the N₁-H bond dissociation in 2⁺. The PES exhibits a steep energy increase up to $d(\text{N}_1\text{-H}) = 2.3 \text{ \AA}$, at which bond length the energy of the system exceeds the threshold energy for 1⁺ + H[•] by 37 kJ mol⁻¹. Unfortunately, gradient optimization at $d(\text{N}_1\text{-H})$ beyond 2.3 Å resulted in highly exothermic H atom migration to C₂, which made it difficult to investigate the singlet PES at large N₁-H separations. The exothermic collapse by H atom migration is prevented on the PES of triplet 2⁺, which shows crossing with the singlet PES at ~2.15 Å which is about 12 kJ mol⁻¹ above the dissociation threshold. Note that at this separation the N₁-H bond is practically interrupted so that the total spin (S^2) of the 1⁺ + H[•] system is no longer a good quantum number, which should facilitate the transition. A similar situation is encountered with the dissociation of the N₃-H bond in 3⁺ (Figure 7b), where the singlet and triplet PESs coalesce at $d(\text{N}_1\text{-H}) = 2.2 \text{ \AA}$. The energy of the coalescence point is ~15 kJ mol⁻¹ above the thermochemical threshold for 1⁺ + H.

The C₂-H bond dissociation in 2⁺ also shows a steep increase in energy that continues to large C₂-H separations (3.0 Å), at which distance the singlet-state energy is 92 kJ mol⁻¹ above that of the products, 9⁺ + H[•] (Figure 8). However, investigation with CASSCF(6,6)/6-31++G(d,p) of the C₂-H dissociation shows a PES that converges to the threshold energy of the products as defined by the asymptote of the triplet state (Figure 8) but without going through a saddle point. This implies a very small activation energy for the addition of an H atom to the C₂ position in distonic ion 9⁺ and likewise for 13⁺. The triplet PES shows a shallow increase in energy up to the transition

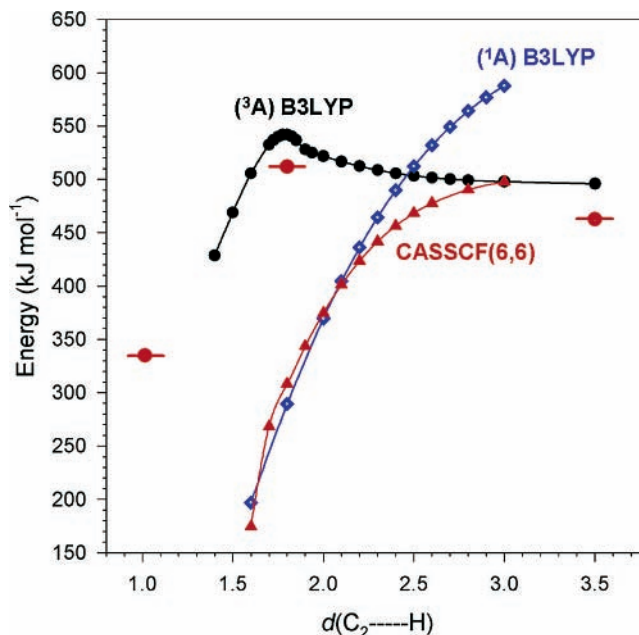


Figure 8. Singlet and triplet potential energy profiles for C₂-H bond dissociation in 2⁺. Diamonds, singlet state by B3LYP; full circles, triplet state by B3LYP; triangles: singlet state by CASSCF(6,6); circles with bars, relative energies of reactant 2⁺, transition state, and products (9⁺ + H[•]) including ZPVE corrections.

state at 1.792 Å, which is 512 kJ mol⁻¹ above 2⁺ and 49 kJ mol⁻¹ above the dissociation threshold (Figure 8).

A comparison of the dissociation and PES energies reveals that the N-H and C-H bond dissociations of 2⁺-4⁺ are mainly determined by the dissociation endothermicities. We conclude that adenine cation radical 1⁺ is the most likely product of dissociation of protonated adenine by the loss of an H atom.

The CAD spectra of protonated adenine isotopomers can be explained by hydrogen migrations prior to the loss of H. These are facilitated by the high threshold energies for the formation of 1⁺. The incomplete scrambling of hydrogen atoms in dissociating adenine ions can be due to the population of high excited states upon collisional excitation at keV energies that results in a fraction of adenine ions in which N-H and C-H bond dissociations are faster than hydrogen migration.

A question arises as to what drives such a highly endothermic H atom loss from protonated adenine tautomers. Because energy transfer in CAD at keV laboratory collision energies occurs on the time scale of a few femtoseconds, electronic excitation in the fast ion is usually considered. We have addressed by time-dependent DFT the singlet and triplet excited-state energies in 2⁺ and 4⁺ to compare the excitation energies with the N-H and C-H bond dissociation energies. The data represent vertical excitation energies from optimized singlet and triplet cations. The results are summarized in Table 4.

The data indicate that collisional excitation in 2⁺ to the first singlet excited state (S_1) supplies sufficient energy (4.89 eV) to drive the dissociation of the N₁-H and N₁₀-H bonds that require 4.22 and 4.39 eV, respectively. In contrast, the dissociation of the C₂-H and C₈-H bonds requires excitation to the S_2 and higher singlet states. On the triplet-state energy manifold, the T_1 state is bound with respect to N-H and C-H bond dissociation, and the higher states are potentially dissociative. However, a singlet-triplet excitation in 2⁺ can be expected to have a low probability of occurring in a single collision and thus can be considered to be an insignificant contributor to highly endothermic dissociations.

TABLE 4: Excited State Energies in 2⁺–4⁺

| cation | state | ΔE_{exc}^a | state | ΔE_{exc}^a | bond | dissociation threshold ^b |
|---------------------|----------------|---------------------------|----------------|---------------------------|--------------------|-------------------------------------|
| (1A) 2 ⁺ | S ₁ | 4.89 | T ₁ | 3.95 | N ₁ –H | 4.22 |
| | S ₂ | 5.06 | T ₂ | 4.96 | N ₁₀ –H | 4.39 |
| | S ₃ | 5.08 | T ₃ | 5.44 | C ₂ –H | 4.79 |
| | S ₄ | 5.19 | T ₄ | 5.47 | C ₈ –H | 5.06 |
| | S ₅ | 6.04 | | | | |
| (1A) 3 ⁺ | S ₁ | 4.79 | T ₁ | 3.32 | N ₃ –H | 4.15 |
| | S ₂ | 5.06 | T ₂ | 4.31 | C ₂ –H | 4.71 |
| | S ₃ | 5.27 | T ₃ | 4.70 | N ₁₀ –H | 4.96 |
| | S ₄ | 5.42 | T ₄ | 4.85 | C ₈ –H | 5.06 |
| | S ₅ | 6.04 | | | | |
| (1A) 4 ⁺ | S ₁ | 4.17 | T ₁ | 3.17 | N ₇ –H | 3.87 |
| | S ₂ | 4.24 | T ₂ | 4.07 | C ₂ –H | 4.33 |
| | S ₃ | 5.22 | T ₃ | 4.24 | C ₈ –H | 4.68 |
| | S ₄ | 5.22 | T ₄ | 4.50 | | |
| | S ₅ | 6.04 | | | | |

^a TD-B3LYP/6-311++G(2d,p) energies in units of electronvolts (eV) relative to the singlet ground state (S₀) energy. ^b B3-PMP2/6-311++G(2d,p) energies relative to the S₀ state of the reactant and including zero-point energy corrections.

The first singlet excited states (S₁) in 3⁺ and 4⁺ are above the lowest dissociation thresholds for the respective N₃–H and N₇–H bond dissociations (Table 4). Dissociations of the C₂–H, C₈–H, and N₁₀–H bonds require excitation into higher states to provide the requisite internal energy in 3⁺ and 4⁺. These results indicate that 3⁺ and 4⁺ may exhibit somewhat greater specificity in CAD to break the respective N–H bonds than does 2⁺.

Adenine Cation Radicals in Aqueous Solution. Polar solvents are known to affect the relative stabilities of nucleobase tautomers greatly, as studied for both stable molecules⁴⁰ and transient open-shell intermediates.⁴⁸ Adenine cation radicals are presumed to be formed transiently in aqueous solution upon pulse radiolysis, and their reactivity is therefore of considerable interest.¹⁶ Table 2 summarizes the calculated relative free energies in aqueous solution of several tautomeric adenine cation radicals. Solvation by bulk water has the effect on the stabilities

of cation radicals 7⁺–14⁺ that all show greater solvation free energies compared to that of 1⁺. This effect is greatest for distonic ion 13⁺, which gains 35 kJ mol⁻¹ of stabilization in water compared to its relative free energy in the gas phase. Nevertheless, the relative free energies of the tautomers in water show 1⁺ to be the most stable adenine cation radical, and the free energy difference between it and the second most stable ion, 6⁺ (14 kJ mol⁻¹ at 298 K), indicates that 1⁺ should be the dominant (>99.5%) tautomer at equilibrium in water.

The reaction of 1⁺ by proton transfer to water was also studied computationally with the goal of identifying which acidic protons in the adenine cation radical may be involved. The calculated free energies for proton transfer are summarized in Table 5, which also shows the structures of the adenine radicals formed. The CCSD(T)/6-311++G(3df,2p) reaction free energies in the gas phase, $\Delta G_{\text{rxn},298}(\text{g})$, and the solvation free energies for the reactants and products in Table 5 were combined according to eq 2 to obtain the reaction free energies in aqueous solution, $\Delta G_{\text{rxn},298}(\text{w})$, where ΔG_{solv} is the change in the solvation free energy as calculated by a PCM scheme (e.g., eq 3 for deprotonation at N₉ forming radical 18 and likewise for the reactions of 1⁺ with OH⁻ (Table 5)).

$$\Delta G_{\text{rxn},298}(\text{w}) = \Delta G_{\text{rxn},298}(\text{g}) + \Delta G_{\text{solv}} \quad (2)$$

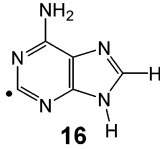
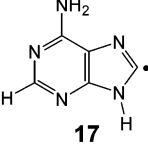
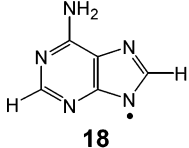
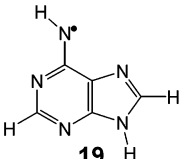
$$\Delta G_{\text{solv}} = \Delta G_{\text{solv}}(\mathbf{18}) + \Delta G_{\text{solv}}(\text{H}_3\text{O}^+) - \Delta G_{\text{solv}}(\mathbf{1}^+) - \Delta G_{\text{solv}}(\text{H}_2\text{O}) \quad (3)$$

$$\text{p}K_{\text{a}} = -\log\{K_{\text{eq}}[\text{H}_2\text{O}]\} = -\log K_{\text{eq}} - 1.744 \quad (4)$$

The $\Delta G_{\text{rxn},298}(\text{w})$ values were used to calculate equilibrium constants (K_{eq}) and $\text{p}K_{\text{a}}$ values for the acidic protons in 1⁺ at high dilution in 55.51 M water (eq 4).

We find that the PCM solvation models give rather large errors for the solvation free energies of H₃O⁺ and OH⁻, so we used the respective experimental values (–435 and –443 kJ

TABLE 5: Acid-Base Reactions of the Adenine Cation Radical in Water

| | reaction | $\Delta G_{298}(\text{w})$ | $\text{p}K_{\text{a}}$ |
|---|--|---------------------------------|-------------------------------------|
|  16 | 1 ⁺ + H ₂ O → 16 + H ₃ O ⁺ | 55 ^a 55 ^b | 7.9 ^a 7.9 ^b |
| | 16 + H ₂ O → 1 ⁺ + OH ⁻ | 63 ^a 64 ^b | 4.6 ^a 4.6 ^b |
|  17 | 1 ⁺ + H ₂ O → 17 + H ₃ O ⁺ | 84 ^a 94 ^b | 12.9 ^a 14.7 ^b |
| | 17 + H ₂ O → 1 ⁺ + OH ⁻ | 35 ^a 25 ^b | 10.4 ^a 9.6 ^b |
|  18 | 1 ⁺ + H ₂ O → 18 + H ₃ O ⁺ | 24 ^a 23 ^b | 2.4 ^a 2.3 ^b |
| | 18 + H ₂ O → 1 ⁺ + OH ⁻ | 66 ^a 66 ^b | 4.2 ^a 4.1 ^b |
|  19 | 1 ⁺ + H ₂ O → 19 + H ₃ O ⁺ | 43 ^a 35 ^b | 3.9 ^a 5.8 ^b |
| | 19 + H ₂ O → 1 ⁺ + OH ⁻ | 75 ^a 83 ^b | 2.5 ^a 1.1 ^b |

^a From CCSD(T) relative energies and solvation free energies using the older PCM model of Tomasi et al.^{31a} ^b From CCSD(T) relative energies and solvation free energies using the refined PCM model of Cossi et al.^{31b}

$\text{mol}^{-1})^{31b}$ instead of the PCM values. The N_9 and N_{10} protons are calculated to be the most acidic in $\mathbf{1}^{+\bullet}$, forming the respective imine radicals $\mathbf{18}$ and $\mathbf{19}$ upon proton transfer to water. The $\text{p}K_a$ values that were calculated by the two PCM schemes using proton transfer to water and OH^- differed somewhat because of uncertainties in the ΔG_{soln} values. We observed recently that averaging the $\text{p}K_a$ from proton transfer to water and OH^- resulted in improved accuracy through error cancellation.⁴⁸ Applying the same correction to the data in Table 5 gives a $\text{p}K_a$ ordering of 3.2, 3.3, 6.2, and 11.9 for the deprotonation of $\mathbf{1}^{+\bullet}$ at N-9, N-10, C-2, and C-8, respectively. Although direct comparison with experimental data is not available for $\mathbf{1}^{+\bullet}$, spectroscopic measurements of the acidity of the 2'-deoxy-adenosine cation radical estimated its $\text{p}K_a$ to be <1 .^{16b} We note in this context that protonated adenosine is about an order of magnitude more acidic than protonated adenine.⁴⁹

The present findings have potentially important implications for the reactivity of the ionized adenine residue in adenosine, DNA, and RNA, where of course the N_9 proton is absent. According to the present calculations, the adenine residue in cation radicals derived from adenosine should be sufficiently acidic to deprotonate at the amine group at physiological pH. The deprotonation of $\mathbf{1}^{+\bullet}$ could be further enhanced by Watson–Crick pairing to thymine (uracil in RNA), which can be expected to facilitate proton transfer from the adenine amine group. Interestingly, the hydrogen atom affinity of N-10 in imine radical $\mathbf{19}$ formed by the deprotonation of $\mathbf{1}^{+\bullet}$ ($-\Delta H_{\text{rxn},0}(\text{g})(\mathbf{19}) = 415 \text{ kJ mol}^{-1}$, $-\Delta G_{\text{rxn},298}(\text{w})(\mathbf{19}) = 383 \text{ kJ mol}^{-1}$) is insufficient for it to abstract a hydrogen atom from the uracil ring in uridine, where breaking the $\text{N}_3\text{-H}$, $\text{C}_5\text{-H}$, and $\text{C}_6\text{-H}$ bonds requires $\Delta H_0(\text{g}) = 497, 477$, and 451 kJ mol^{-1} , respectively.⁵⁰ However, the hydrogen atom affinity of the iminyl nitrogen (N-10) in $\mathbf{19}$ is sufficient for an exothermic hydrogen transfer from the methyl group in thymine or from other hydrogen atom donors, such as the SH group in cysteine, the OH group in tyrosine, or C_α methines of the peptide backbone.^{51,52}

Conclusions

The collisionally activated dissociation of protonated adenine tautomers proceeds by the highly endothermic loss of a hydrogen atom. The lowest-energy product, which is also preferred kinetically, is the adenine cation radical ($\mathbf{1}^{+\bullet}$). The loss of H is triggered by the formation upon collisional activation of an excited singlet state in the dissociating cation. Adenine cation radical $\mathbf{1}^{+\bullet}$ is calculated to be the most stable tautomer in aqueous solution. The primary reactivity of $\mathbf{1}^{+\bullet}$ in water is proton transfer to the solvent, which involves the most acidic N_9 and amine protons in adenine. Deprotonation at the amino group is postulated as the energetically most favorable acid–base reaction of the adenine cation radical in RNA and DNA that produces highly reactive adenine imine radicals that can further react by exothermic hydrogen atom abstraction from suitable donors such as thymine, cysteine, and tyrosine side chains or the C_α methines of a peptide backbone.

Acknowledgment. Support of this work by the National Science Foundation (grant CHE-0349595 for experiments and CHE-0342956 for computations) is gratefully acknowledged. E.A.S. thanks the Alma and Lloyd West Graduate Student Fellowship for support during the course of this work. P.G. thanks the Fonds National pour la Recherche Scientifique for financial support in the acquisition of the Micromass AutoSpec 6F mass spectrometer and for continuing support. M.T.N. thanks the Department of Chemistry at the University of Washington

for warm hospitality and support during his stay in the summer of 2002. The JEOL HX-100 mass spectrometer used in this study was a generous donation from the former Biomembrane Institute, Seattle, Washington, courtesy of Professor S. Hakomori.

Supporting Information Available: Tables S1–S15 with B3LYP/6-31+G(d,p) and B3LYP/6-311++G(d,p) optimized geometries in Cartesian coordinate format and Figures S1–S4 with molecular orbitals. This material is available free of charge via the Internet at <http://pubs.acs.org>.

References and Notes

- (1) (a) Hammerum, S. *Mass Spectrom. Rev.* **1988**, *7*, 123–202. (b) Stirk, K. M.; Kiminkinen, L. K. M.; Kentamaa, H. I. *Chem. Rev.* **1992**, *92*, 1649–1665.
- (2) (a) Tureček, F.; Smutek, M.; Hanuš, V. *Org. Mass Spectrom.* **1981**, *16*, 483–489. For a comprehensive review, see (b) Grützmaier, H.-F. *Int. J. Mass Spectrom. Ion Processes* **1992**, *118/119*, 825–855.
- (3) Yates, B. F.; Bouma, W.; Radom, L. *J. Am. Chem. Soc.* **1984**, *106*, 5805–5808.
- (4) Yates, B. F.; Bouma, W.; Radom, L. *J. Am. Chem. Soc.* **1987**, *109*, 2250–2263.
- (5) (a) Flammang, R.; Barbieux-Flammang, M.; Gualano, E.; Gerbaux, P.; Le, H. T.; Nguyen, M. T.; Tureček, F.; Vivekananda, S. *J. Phys. Chem. A* **2001**, *105*, 8579–8587. (b) Flammang, R.; Flammang-Barbieux, M.; Gualano, E.; Gerbaux, P.; Le, H. T.; Nguyen, M. T.; Tureček, F. *Int. J. Mass Spectrom.* **2002**, *217*, 65–73.
- (6) (a) Lavorato, D. J.; Terlouw, J. K.; Dargel, T. K.; Koch, W.; McGibbon, G. A.; Schwarz, H. *J. Am. Chem. Soc.* **1996**, *118*, 11898–11904. (b) Lavorato, D. J.; Terlouw, J. K.; McGibbon, G. A.; Dargel, T. K.; Koch, W.; Schwarz, H. *Int. J. Mass Spectrom.* **1998**, *179/180*, 7–14. (c) Lavorato, D. J.; Fell, L. M.; McGibbon, G. A.; Sen, S.; Terlouw, J. K.; Schwarz, H. *Int. J. Mass Spectrom.* **2000**, *195/196*, 71–83.
- (7) Lavorato, D. J.; Dargel, T. K.; Koch, W.; McGibbon, G. A.; Schwarz, H.; Terlouw, J. K. *Int. J. Mass Spectrom.* **2001**, *210/211*, 43–57.
- (8) Dargel, T. K.; Koch, W.; Lavorato, D. J.; McGibbon, G. A.; Terlouw, J. K.; Schwarz, H. *Int. J. Mass Spectrom.* **1999**, *185/186/187*, 925–933.
- (9) McGibbon, G. A.; Heinemann, C.; Lavorato, D. J.; Schwarz, H. *Angew. Chem., Int. Ed. Engl.* **1997**, *36*, 1478–1481.
- (10) McGibbon, G. A.; Hrusak, J.; Lavorato, D. J.; Schwarz, H.; Terlouw, J. K. *Chem.—Eur. J.* **1997**, *3*, 232–236.
- (11) Karni, A.; Mandelbaum, A. *Org. Mass Spectrom.* **1980**, *15*, 53–57.
- (12) McLafferty, F. W.; Tureček, F. *Interpretation of Mass Spectra*, 4th ed.; University Science Books: Sausalito, CA, 1993; pp 55, 176.
- (13) Šponar, J.; Hobza, P. *Collect. Czech. Chem. Commun.* **2003**, *68*, 2231–2282.
- (14) Improta, R.; Scalmani, G.; Barone, V. *Int. J. Mass Spectrom.* **2000**, *201*, 321–336.
- (15) Li, X.; Cai, Z.; Sevilla, M. D. *J. Phys. Chem. A* **2002**, *106*, 9345–9351.
- (16) (a) Steenken, S.; Jovanovic, S. V. *J. Am. Chem. Soc.* **1997**, *119*, 617–618. (b) Steenken, S. *Biol. Chem.* **1997**, *378*, 1293–1297. (c) Steenken, S. *Chem. Rev.* **1989**, *89*, 503–520. (d) Steenken, S. *Free Radical Res. Commun.* **1992**, *16*, 349–379.
- (17) (a) Crespo-Hernandez, C. E.; Martinez, L.; Gonzalez-Sierra, A. E.; Robles-Irizarry, L.; Diaz-Vazquez, A.; Arce, R. J. *Photochem. Photobiol., A* **2002**, *152*, 123–133. (b) Reynisson, J.; Steenken, S. *Phys. Chem. Chem. Phys.* **2002**, *4*, 527–532. (c) Sartor, V.; Boone, E.; Schuster, G. B. *J. Phys. Chem. B* **2001**, *105*, 11057–11059. (d) Bertran, J.; Oliva, A.; Rodriguez-Santiago, L.; Sodupe, M. *J. Am. Chem. Soc.* **1998**, *120*, 8159–8167. (e) Hutter, M.; Clark, T. *J. Am. Chem. Soc.* **1996**, *118*, 7574–7577. (f) Faraggi, M.; Ferradini, C.; Jay-Gerin, J.-P. *New J. Chem.* **1995**, *19*, 1203–1215. (g) Al-Sheikhly, M. *Radiat. Phys. Chem.* **1994**, *44*, 297–301. (h) Nelson, W. H.; Sagstuen, E.; Hole, E. O.; Close, D. M. *Radiat. Res.* **1992**, *131*, 272–284. (i) Yan, M.; Becker, D.; Summerfield, S.; Renke, P.; Sevilla, M. D. *J. Phys. Chem.* **1992**, *96*, 1983–1989. (j) Candeias, L. P.; O'Neill, P.; Jones, G. D. D.; Steenken, S. *Int. J. Radiat. Biol.* **1992**, *61*, 15–20. (k) Sevilla, M. D.; Becker, D.; Yan, M.; Summerfield, S. R. *J. Phys. Chem.* **1991**, *95*, 3409–3415. (l) Sevilla, M. D.; Mohan, P. A. *Int. J. Radiat. Biol.* **1974**, *25*, 635–638. (m) Nelson, W. H.; Sagstuen, E.; Hole, E. O.; Close, D. M. *Radiat. Res.* **1992**, *131*, 272–284.
- (18) Laxer, A.; Major, D. T.; Gottlieb, H. E.; Fischer, B. *J. Org. Chem.* **2001**, *66*, 5463–5481.
- (19) Bateman, R. H.; Brown, J.; Lefevre, M.; Flammang, R.; Van Haverbeke, Y. *Int. J. Mass Spectrom. Ion Processes* **1992**, *115*, 205–218.
- (20) (a) Frisch, M. J.; Trucks, G. W.; Schlegel, H. B.; Scuseria, G. E.; Robb, M. A.; Cheeseman, J. R.; Zakrzewski, V. G.; Montgomery, J. A.,

- Jr.; Stratmann, R. E.; Burant, J. C.; Dapprich, S.; Millam, J. M.; Daniels, A. D.; Kudin, K. N.; Strain, M. C.; Farkas, O.; Tomasi, J.; Barone, V.; Cossi, M.; Cammi, R.; Mennucci, B.; Pomelli, C.; Adamo, C.; Clifford, S.; Ochterski, J.; Petersson, G. A.; Ayala, P. Y.; Cui, Q.; Morokuma, K.; Malick, D. K.; Rabuck, A. D.; Raghavachari, K.; Foresman, J. B.; Cioslowski, J.; Ortiz, J. V.; Stefanov, B. B.; Liu, G.; Liashenko, A.; Piskorz, P.; Komaromi, I.; Gomperts, R.; Martin, R. L.; Fox, D. J.; Keith, T.; Al-Laham, M. A.; Peng, C. Y.; Nanayakkara, A.; Gonzalez, C.; Challacombe, M.; Gill, P. M. W.; Johnson, B. G.; Chen, W.; Wong, M. W.; Andres, J. L.; Head-Gordon, M.; Replogle, E. S.; Pople, J. A. *Gaussian 98*, revision A.6; Gaussian, Inc.: Pittsburgh, PA, 1998. (b) Frisch, M. J.; Trucks, G. W.; Schlegel, H. B.; Scuseria, G. E.; Robb, M. A.; Cheeseman, J. R.; Montgomery, J. A., Jr.; Vreven, T.; Kudin, K. N.; Burant, J. C.; Millam, J. M.; Iyengar, S. S.; Tomasi, J.; Barone, V.; Mennucci, B.; Cossi, M.; Scalmani, G.; Rega, N.; Petersson, G. A.; Nakatsuji, H.; Hada, M.; Ehara, M.; Toyota, K.; Fukuda, R.; Hasegawa, J.; Ishida, M.; Nakajima, T.; Honda, Y.; Kitao, O.; Nakai, H.; Klene, M.; Li, X.; Knox, J. E.; Hratchian, H. P.; Cross, J. B.; Adamo, C.; Jaramillo, J.; Gomperts, R.; Stratmann, R. E.; Yazyev, O.; Austin, A. J.; Cammi, R.; Pomelli, C.; Ochterski, J. W.; Ayala, P. Y.; Morokuma, K.; Voth, G. A.; Salvador, P.; Dannenberg, J. J.; Zakrzewski, V. G.; Dapprich, S.; Daniels, A. D.; Strain, M. C.; Farkas, O.; Malick, D. K.; Rabuck, A. D.; Raghavachari, K.; Foresman, J. B.; Ortiz, J. V.; Cui, Q.; Baboul, A. G.; Clifford, S.; Cioslowski, J.; Stefanov, B. B.; Liu, G.; Liashenko, A.; Piskorz, P.; Komaromi, I.; Martin, R. L.; Fox, D. J.; Keith, T.; Al-Laham, M. A.; Peng, C. Y.; Nanayakkara, A.; Challacombe, M.; Gill, P. M. W.; Johnson, B. G.; Chen, W.; Wong, M. W.; Gonzalez, C.; Pople, J. A. *Gaussian 03*, revision B.05; Gaussian, Inc.: Pittsburgh, PA, 2003.
- (21) (a) Becke, A. D. *J. Chem. Phys.* **1993**, *98*, 1372–1377. (b) Becke, A. D. *J. Chem. Phys.* **1993**, *98*, 5648–5652. (c) Stephens, P. J.; Devlin, F. J.; Chabalowski, C. F.; Frisch, M. J. *J. Phys. Chem.* **1994**, *98*, 11623–11627.
- (22) (a) Schlegel, H. B. *J. Chem. Phys.* **1986**, *84*, 4530–4534. (b) Mayer, I. *Adv. Quantum Chem.* **1980**, *12*, 189–262.
- (23) Tureček, F. *J. Phys. Chem. A* **1998**, *102*, 4703–4713.
- (24) (a) Rablen, P. R.; Bentrup, K. H. *J. Am. Chem. Soc.* **2003**, *125*, 2142–2147. (b) Rablen, P. R. *J. Org. Chem.* **2000**, *65*, 7930–7937. (c) Rablen, P. R. *J. Am. Chem. Soc.* **2000**, *122*, 357–368.
- (25) (a) Tureček, F.; Wolken, J. K. *J. Phys. Chem. A* **1999**, *103*, 1905–1912. (b) Wolken, J. K.; Tureček, F. *J. Am. Chem. Soc.* **1999**, *121*, 6010–6018. (c) Wolken, J. K.; Tureček, F. *J. Phys. Chem. A* **1999**, *103*, 6268–6281. (d) Tureček, F.; Carpenter, F. H.; Polce, M. J.; Wesdemiotis, C. *J. Am. Chem. Soc.* **1999**, *121*, 7955–7956. (e) Tureček, F.; Poláček, M.; Frank, A. J.; Sadílek, M. *J. Am. Chem. Soc.* **2000**, *122*, 2361–2370.
- (26) Poláček, M.; Tureček, F. *J. Am. Chem. Soc.* **2000**, *122*, 9511–9524.
- (27) Čížek, J.; Paldus, J.; Šroubková, L. *Int. J. Quantum Chem.* **1969**, *3*, 149–167.
- (28) Purvis, G. D.; Bartlett, R. J. *J. Chem. Phys.* **1982**, *76*, 1910–1918.
- (29) Reed, A. E.; Weinstock, R. B.; Weinhold, F. *J. Chem. Phys.* **1985**, *83*, 735–746.
- (30) (a) Hegarty, D.; Robb, M. A. *Mol. Phys.* **1979**, *38*, 1795–1812. (b) Frisch, M.; Ragazos, I. N.; Robb, M. A.; Schlegel, H. B. *Chem. Phys. Lett.* **1992**, *189*, 524–528.
- (31) (a) Barone, V.; Cossi, M.; Tomasi, J. *J. Chem. Phys.* **1997**, *107*, 3210–3221. (b) Cossi, M.; Scalmani, G.; Rega, N.; Barone, V. *J. Chem. Phys.* **2002**, *117*, 43–54.
- (32) Major, D. T.; Laxer, A.; Fischer, B. *J. Org. Chem.* **2002**, *67*, 790–802.
- (33) For recent studies of protonation sites in heterocycles and nucleobases, see (a) Wolken, J. K.; Syrstad, E. A.; Vivekananda, S.; Tureček, F. *J. Am. Chem. Soc.* **2001**, *123*, 5804–5805. (b) Wolken, J. K.; Tureček, F. *J. Phys. Chem. A* **2001**, *105*, 8352–8360. (c) Wolken, J. K.; Tureček, F. *J. Am. Soc. Mass Spectrom.* **2000**, *11*, 1065–1071. (d) Wolken, J. K.; Tureček, F. *J. Am. Chem. Soc.* **1999**, *121*, 6010–6018. (e) Nguyen, V. Q.; Tureček, F. *J. Am. Chem. Soc.* **1997**, *119*, 2280–2290. (f) Nguyen, V. Q.; Tureček, F. *J. Mass Spectrom.* **1997**, *32*, 55–63. (g) Nguyen, V. Q.; Tureček, F. *J. Mass Spectrom.* **1996**, *31*, 1173–1184.
- (34) Hunter, E. P.; Lias, S. G. *J. Phys. Chem. Ref. Data* **1998**, *27*, 413.
- (35) Podolyan, Y.; Gorb, L.; Leszczynski, J. *J. Phys. Chem. A* **2000**, *104*, 7346–7352.
- (36) Harrison, A. G. *Chemical Ionization Mass Spectrometry*, 2nd ed.; CRC Press: Boca Raton, FL, 1992; p 30.
- (37) (a) Wolken, J. K.; Syrstad, E. A.; Vivekananda, S.; Tureček, F. *J. Am. Chem. Soc.* **2001**, *123*, 5804–5805. (b) Syrstad, E. A.; Vivekananda, S.; Tureček, F. *J. Phys. Chem. A* **2001**, *105*, 8339–8351.
- (38) Seymour, J. L.; Syrstad, E. A.; Langley, C. C.; Tureček, F. *Int. J. Mass Spectrom.* **2003**, *228*, 687–702.
- (39) (a) Thoelmann, D.; Grutzmacher, H.-F. *J. Am. Chem. Soc.* **1991**, *113*, 3281–3287. (b) Nixdorf, A.; Grutzmacher, H.-F. *J. Am. Chem. Soc.* **1997**, *119*, 6544–6551.
- (40) Hanus, M.; Kabeláč, M.; Rejnek, J.; Ryjáček, F.; Hobza, P. *J. Phys. Chem. B* **2004**, *108*, 2087–2097.
- (41) Orlov, V. M.; Smirnov, A. N.; Varshavsky, Y. M. *Tetrahedron Lett.* **1976**, *48*, 4377–4378.
- (42) Hush, N. S.; Cheung, A. S. *Chem. Phys. Lett.* **1975**, *34*, 11–13.
- (43) Lin, J.; Yu, C.; Peng, S.; Akiyama, I.; Li, K.; Lee, L. K.; LeBreton, P. R. *J. Am. Chem. Soc.* **1980**, *102*, 4627–4631.
- (44) Hwang, C. T.; Stumpf, C. L.; Yu, Y.-Q.; Kenttamaa, H. I. *Int. J. Mass Spectrom.* **1999**, *182/183*, 253–259.
- (45) Additional calculations of the adenine adiabatic ionization energy with effective CCSD(T)/6-311++G(3df,2p) + ZPVE gave $IE_{\text{adiab}} = 8.25$ eV in excellent agreement with both the photoionization and B3-PMP2-calculated values.
- (46) Gerbaux, P. Unpublished results.
- (47) Armentrout, P. B.; Simons, J. *J. Am. Chem. Soc.* **1992**, *114*, 8627–8633.
- (48) Tureček, F.; Yao, C. *J. Phys. Chem. A* **2003**, *107*, 9221–9231.
- (49) Christensen, J. J.; Rytting, J. H.; Izatt, R. M. *Biochemistry* **1970**, *9*, 4907–4913.
- (50) Tureček, F.; Wolken, J. K. *J. Phys. Chem. A* **2001**, *105*, 8740–8747.
- (51) Rauk, A.; Yu, D.; Armstrong, D. A. *J. Am. Chem. Soc.* **1998**, *120*, 8848–8855.
- (52) Rauk, A.; Yu, D.; Taylor, J.; Shustov, G. V.; Block, D. A.; Armstrong, D. A. *Biochemistry* **1999**, *38*, 9089–9096.